Enhancing Joint Dynamics Modeling for Underwater Robotics Through Stochastic Extension

Mingxuan Ding, Gang Wang, *Senior Member, IEEE*, Lingzhe Meng, Jixin Wang, Liquan Wang, Dake Lu, Junlong Wang, Feihong Yun, and Peng Jia

***Abstract*—Accurate joint dynamics models are essential for the compliance and robustness of robot control, especially for robots operating in complex underwater environments. To improve the precision of joint dynamics models, much research focuses on refining specific parameters or incorporating previously overlooked parameters through theoretical deductions and simulations. However, the effectiveness of these advancements can only be determined through empirical validation using the new model. This letter delineates a methodology that facilitates the assessment of potential avenues for enhancing the model, without necessitating prior theoretical derivation. Specifically, a methodology based on stochastic extension is proposed for evaluating directions of model improvement, applied to enhancing the LuGre model for underwater sealed joints. This approach employs the coefficient of variation in LuGre model parameters to assess the direction of model enhancement, with the comparison of coefficients of variation before and after improvement elucidating the superiority of the enhancements. Experimental outcomes corroborate that the LuGre model, refined using this evaluative technique, can precisely estimate friction forces across diverse typical conditions in underwater joint applications. The sealed joints utilizing the improved model demonstrated enhanced response times and precision in underwater environments.**

***Index Terms*—Marine robotics, dynamics, contact modeling.**

I. Introduction

As UNDERWATER robotics evolve, the demand for precise modeling of high-performance underwater actuated joints grows. These joints are crucial for robots operating in various underwater environments, such as legged and wheeled robots, and near-wall environments [1]. Unlike traditional thrusters, these robots rely on high-performance underwater actuated joints to perceive interactions for gait and posture selection in legged robots and torque outputs for control in wheeled robots. Therefore, establishing accurate mappings between input and output for underwater actuated joints is crucial.

The primary focus and challenge in joint modeling lie in the identification of friction models [2]. Friction, responsible for nearly 30% of the world's primary energy consumption [3], exerts an even more significant influence on driving joints.The complexity of friction far surpasses that of classical linear friction models, with the Stribeck effect showcasing the non-linear relationship between friction and velocity [4]. This non-linearity poses significant challenges in mapping joint inputs to outputs, ultimately determining the control and functional limits of robots [5]. This has resulted in the development of friction models, such as the Dahl's model, LuGre model, and others, which serve as an essential link between observable data and dynamic friction in joints during robot motion.

The LuGre model, known for its comprehensive depiction of friction characteristics, serves as a benchmark for small-scale actuated joint dynamics [6]. An extension of Dahl's model, the LuGre model effectively captures the Stribeck effect and accurately describes complex frictional behaviors such as stick-slip motion and friction hysteresis. As a foundational model in mechanical servo systems, Dahl's model has been widely accepted and utilized for simulating friction in various systems, including aerospace applications [7]. The LuGre model builds on the bristle model. It sees the frictional interface as two rigid bodies in contact through an array of elastic bristles. This extends and refines Dahl's model, yielding better results. Despite its widespread use, the LuGre model may lack stability or accuracy in certain operating conditions [8], leading to ongoing model enhancements by refining or adding parameters [9], [10].

While many studies aim to improve the LuGre model, there is currently no established method for determining the direction of improvement, especially for underwater actuated joint modeling. The non-rigid contact of underwater drive joints, resulting from their sealing components, renders their friction characteristics highly sensitive to external influences [11], [12]. Existing enhancement methods lack universal validation across all conditions, requiring a meticulous process of theoretical analysis and experimental testing for model optimization.

This letter introduces a methodology for guiding model enhancements that provides insights into improving the LuGre

Manuscript received 9 April 2024; accepted 2 August 2024. Date of publication 8 August 2024; date of current version 14 August 2024. This article was recommended for publication by Associate Editor Enrico Mingo Hoffman and Editor Lucia Pallottino upon evaluation of the reviewers' comments. This work was supported by the National Key Research and Development Program of China under Grant 2023YFB3407702. *(Corresponding author: Gang Wang.)*

Mingxuan Ding, Lingzhe Meng, Jixin Wang, Liquan Wang, Dake Lu, Feihong Yun, and Peng Jia are with the College of Mechanical and Electrical Engineering, Harbin Engineering University, Harbin 150001, China, and also with the National Key Laboratory of Autonomous Marine Vehicle Technology, Harbin Engineering University, Harbin 150001, China (e-mail: dingmx@hrbeu.edu.cn; menglingzhe@hrbeu.edu.cn; wangjixin1012@hrbeu.edu.cn; wangliquan@hrbeu.edu.cn; lbj990224@hrbeu.edu.cn; yunfeihong@hrbeu.edu.cn; jiapeng@hrbeu.edu.cn).

Gang Wang and Junlong Wang are with the National Key Laboratory of Autonomous Marine Vehicle Technology, Harbin Engineering University, Harbin 150001, China (e-mail: wanggang@hrbeu.edu.cn; wangjunl@hrbeu.edu.cn).

This letter has supplementary downloadable material available at https://doi.org/10.1109/LRA.2024.3440769, provided by the authors.

Digital Object Identifier 10.1109/LRA.2024.3440769

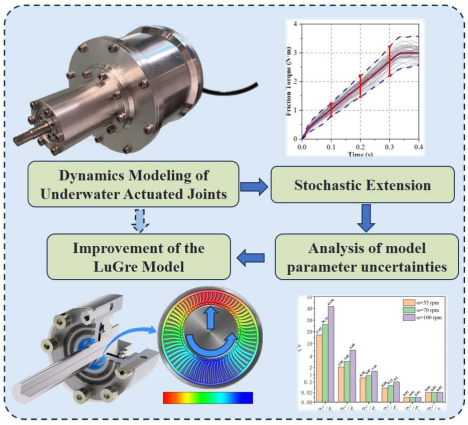

Fig. 1. The proposed method guides the improvement of the model. Model improvement is achieved through the steps of 'randomness expansion – analysis of model parameter uncertainty – specified parameter optimization'.

model utilized in underwater actuated joint dynamics, as depicted in Fig. 1, without the need for prior theoretical derivation. We employ a stochastic extension to quantitatively assess the reliability of the LuGre model's parameters within the defined operational condition range, pointing out directions for improvement. The experimental data obtained can be repeatedly used throughout the model enhancement process, ensuring cost-effective optimization. Utilizing this method, we have refined the LuGre model for underwater joints. The effectiveness of both our model improvement direction evaluation method and the refined model was confirmed through experimental data comparison and model uncertainty analysis, demonstrating a robust solution for challenges like underwater actuated joint modeling.

A. Related Studies

In order to meet the specialized needs of underwater operations, an increasing number of robot designs utilizing high-performance joints are being adapted for underwater environments. Picardi et al. developed an underwater legged robot called "SILVER2," which features six legs, each composed of three underwater joints, to perform tasks such as underwater biological observation [13]. Kim et al. developed a multimodal underwater robot, designated "HERO-BLUE," which employs multiple underwater joints to achieve three modes of locomotion: walking, swimming, and crawling [14]. Ma et al. designed an amphibious robot that utilizes high-performance underwater joints to meet the demands for high torque during crawling and high rotational speed during swimming [15]. Dong et al. equipped a fish-like robot with underwater joint-driven pectoral fins, enabling the robot to escape from stranded situations [16]. While the use of underwater joints is already quite mature, the complex frictional changes caused by the sealing structure and underwater environment prevent the direct application of terrestrial joint friction models to underwater robots, posing significant challenges for robot motion control and functional expansion.

A considerable amount of research has been devoted to improving or adapting the LuGre model to suit different operating conditions. The LuGre model is widely used in engineering, but it oversimplifies observed friction behaviors. This makes it challenging to effectively characterize significant variations in unmodeled variables, such as overload effects [17], frequent reciprocating motions [18], and changes in contact media [19]. These variations can lead to reduced estimation accuracy and instability. A frequently used optimization strategy is to integrate displacement direction and magnitude considerations into the LuGre model [10], [20], [21]. These improvements usually entail redefining the bristle stiffness and damping coefficient of the LuGre model from constant values to linear or nonlinear functions relative to displacement. This results in relatively low computational overhead. Consequently, these improvements can be integrated into motor controllers to provide real-time compensation at the hardware level. Promising results have been shown in systems with linear or reciprocating motion. Some studies have investigated specific contact media under certain conditions to refine the LuGre model [19], [22], such as servo systems operating in environments with magnetic rheology or grease lubrication. These studies aim to improve the accuracy and stability of the LuGre model. They emphasize the importance of acknowledging that the LuGre model may not be universally applicable and may require enhancements. Additionally, they suggest the need for a generalized LuGre enhancement model or a reliable method to guide improvements.

Several studies have attempted to improve the LuGre model in a general sense. These efforts have explored various avenues for enhancement, such as changes in friction surface pressure [23], the impact of dwell time [24], and multidimensional expansions [25]. However, none of these studies have demonstrated universal applicability across all operating conditions. Instead, they have only demonstrated superiority over the original model under specific conditions. Therefore, for emerging challenges such as modeling underwater actuated joints, a reliable method is urgently needed to effectively guide the improvement of the LuGre model.

B. Contributions

The proposed method makes several key contributions to the field:

We propose a new method for evaluating models using probabilistically valid stochastic extensions, offering insights into model enhancement pathways by considering uncertainty.

We introduce an enhanced LuGre model tailored for underwater actuated joints, accurately estimating friction in response to external force variations.

Our improved model, validated through experiments compared to the standard LuGre model, demonstrates accuracy and responsiveness.

II. Improved LuGre Model Under Evaluation of Model Stochastic Extension Method

A. LuGre Model Evaluation Method Based on Stochastic Extension

The LuGre model, derived from Dahl's model, is renowned for capturing the Stribeck effect, making it a benchmark for

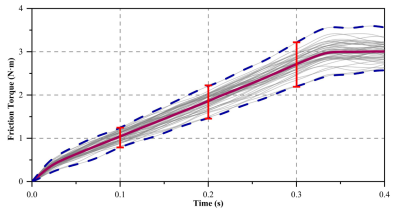

Fig. 2. The friction torque curve of the underwater driving joint under specific operational conditions is depicted. The gray area represents a sample curve derived from 50 experiments, while the blue dashed line indicates the extreme values of all samples at each time point within these conditions. Monitoring points were set at intervals of 0.1 s, 0.2 s, and 0.3 s, with red vertical lines denoting the data range at each moment.

analyzing complex friction phenomena like stick-slip motion. Dahl's model originated from an experiment with a pendulum on ball bearings, resulting in linear amplitude decay and the exponential function formulation. Expanding on Dahl's work, the LuGre model incorporates the bristle model, forming a one-dimensional second-order dynamic model based on average bristle deformation perpendicular to sliding.

$$F = k_0 z + k_1 \dot{z} + k_2 \dot{x}$$

$$\dot{z} = \dot{x} - \frac{k_0 \dot{x}}{g(\dot{x})} z$$

$$g(\dot{x}) = F_C + (F_S - F_C) e^{-(\dot{x}/v_s)^2} \tag{1}$$

Where F represents friction force, x denotes displacement, k_0. represents the stiffness of the bristles, k_1 denotes the damping coefficient of the bristles, k_2 represents the viscous friction coefficient, z represents the average deformation of the bristles, F_S represents static friction, F_C represents Coulomb friction, and v_s represents the Stribeck velocity. After we complete parameter identification, the accuracy of the model can be quantitatively analyzed through friction estimation experiments. However, if the accuracy of the model fails to meet the requirements, existing methods cannot directly provide targeted directions for model improvement. Especially for the particular issue of underwater robots, there are many factors in the working conditions such as underwater pressure, external loads, etc., which may significantly affect the estimation results, further increasing the difficulty of determining improvement directions.

$$g(W,t) = \begin{cases} 0, M_W(t) \subset reg_W(t) \\ 1, M_W(t) \not\subset reg_W(t) \end{cases} \tag{2}$$

The fitting parameters obtained through as comprehensive experiments as possible can be considered as the probability mean under the influence of various variables. By increasing the dimension of parameter uncertainty, we can guide the direction of model improvement. We use the method of probabilistically valid stochastic extensions of deterministic models to increase the information dimension of the model [27]. For the friction model of underwater actuated joints, when we track the velocity using the friction compensation of the LuGre model, due to unconsidered variables, the friction curves obtained from multiple experiments will form a range region, as shown in the red area in Fig. 2. Let a certain type of experiment produce data range $reg_W(t)$ at a certain moment, where W is the corresponding dataset of the experiment. Whether the result $M_W(t)$ generated by the model under this process is in $reg_W(t)$ can be defined by decision function (2).

We can define the probability of deviating from the estimated data $reg_W(t)$ by parameterizing the fit as parameter $\bar{\xi}$ as the probability of violating probability $P(\xi)$.

$$P(\bar{\xi}) = \frac{\sum_{w=0}^{W} g(w,t)}{W} \tag{3}$$

The parameter $P(\bar{\xi})$ partly characterizes the fidelity of the model, representing its accuracy, while on the other hand, it also characterizes the diversity or expressive power of the model. A larger deviation probability implies that the model is prone to generating outlier data, but a very small deviation probability, such as $P(\bar{\xi}) = 0$, although high in accuracy, may be a very conservative model in terms of model diversity. First, uncertainty vectors ψ corresponding to parameters in $\bar{\xi}$ are given. Assuming that the parameters are mutually independent and follow a normal distribution, we can characterize the uncertainty with variance, denoted as $\psi = \{\sigma_0^2, \sigma_1^2, \sigma_2^2, \sigma_3^2, \sigma_4^2, \sigma_5^2\}$. Based on this, we can sample the parameters under the normal distribution to relax certain deviation probabilities as conditions, and define the diversity coefficient α to express the range of model accuracy. (4) provides the mathematical expression.

$$\begin{cases} S = \{\xi \in N(\bar{\xi}, \psi) | P(\xi) \geq P_0\} \\ P_W(S) \leq \alpha \end{cases} \tag{4}$$

The meaning of (4) is to define an acceptable range of model accuracy. Giving a lower bound P_0 for the deviation probability, a smaller α implies that the model fits the real-world joint friction model better. After specifying the range of model accuracy, we expect the model to have the best diversity, i.e., the maximum uncertainty of the model. Based on this, we can define the optimization function (5) to seek the maximum uncertainty, i.e., the best diversity.

$$\max[Tr(Cov(\xi,\xi))], \text{with } P_0(N(\bar{\xi}, \psi), \alpha) \leq \rho \tag{5}$$

$Tr()$ represents the trace of the matrix, and $Cov()$ represents the covariance matrix. Based on (5), it is also necessary to determine the number of samples m in the experiment and the number of samples n for the uncertainty parameters. According to Vidyasagar's conclusion, when we specify the confidence level δ, the number of samples n for the uncertainty parameters should satisfy (6) [28]. Furthermore, when specifying the accuracy ε, (7) can be used to determine the number of samples m for a given n [29].

$$n \geq \frac{\log(2/\delta)}{\log(1/(1-\alpha))} \tag{6}$$

$$m \geq \frac{1}{2\varepsilon^2} 1\text{n}\left(\frac{4n}{\delta}\right) \tag{7}$$

From this, we can determine all the necessary parameters for the experiment. For the optimization problem (4), we only need to sample the confidence interval and use the least squares

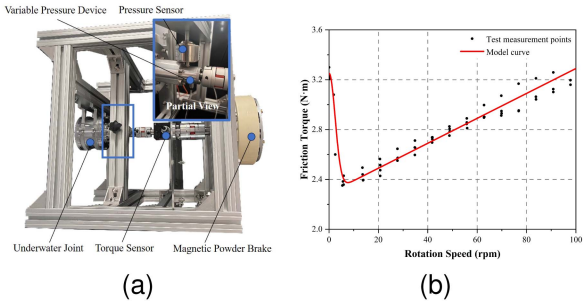

Fig. 3. Test equipment and LuGre model fitting curve. (a) Simulation test device. (b) Friction force estimation curve.

method to maximize the objective function, thereby obtaining the variance vector ψ_R for the given model. As mentioned earlier, the direction of improvement for a model needs to be evaluated using the dimension of uncertainty. For a particular parameter, a larger variance to some extent represents the comprehensiveness of our consideration for that parameter in the model. A larger maximum variance under a given accuracy range indicates a greater impact of variables on this parameter. By comparing the normalized variances of each parameter, we can qualitatively describe the direction of model improvement and evaluate the advantages and disadvantages between two models.

First, the variance in ψ_R can be normalized using the coefficient of variation(CV), and the normalized vector is denoted as ψ_{CV}. By comparing the elements of ψ_{CV}, we can qualitatively determine the optimization direction, i.e., there may be components worth refining. On the other hand, when we compare two models using the same confidence level criteria and accuracy range, we can calculate the sum of the elements in ψ_{CV} for different models, compare the results, and qualitatively judge the superiority or inferiority of the two models. We call this calculated result the cumulative randomness of the model, denoted as $sum(\psi_{CV})$.

$$\psi_{CV} = |\psi_R/\bar{\xi}| \tag{8}$$

B. Stochastic Extension and Evaluation of the LuGre Model

We initially fit LuGre model parameters using the equipment shown in Fig. 3. Equipment parameters are listed in Table I. Torque from the sealing element is considered as the difference between output torque and sensor-measured torque.We employed a method similar to that described in reference [26] to divide the parameters of the LuGre model into two groups: static parameters $\bar{\xi}_s = \{k_0, k_1\}$ and dynamic parameters $\bar{\xi}_d = \{k_2, F_C, F_s, \nu_s\}$ for fitting. The experimental data were used to fit the parameters using the least squares method with a step size of 0.01. Radial loading and underwater pressure simulation were not performed in fitting experiments. The velocity versus friction force curve is depicted in Fig. 4, demonstrating the model's ability to capture the Stribeck effect with an average estimation error of 1.8%, confirming its accuracy.

The LuGre model has six parameters that need to be identified through experiments, and we denote the parameter vector to be

TABLE I
EQUIPMENT AND PARAMETERS

Equipment	Model	Parameters
Underwater joint	-	Sealing method: HBTS, Max operating water depth: 30m, Max output speed: 100rpm, Max output torque: 26Nm
Torque sensor	STBD-S	Range 0∼ 50Nm, accuracy ±0.2Nm
Pressure sensor	DLZS-41	Range 0∼ 100N, accuracy ±0.03N
Magnetic powder brake	Hibles-PB	Generate a resistance torque range of 0∼50Nm.
Variable pressure device	JB 550W	Maximum generated pressure 0.7Mpa

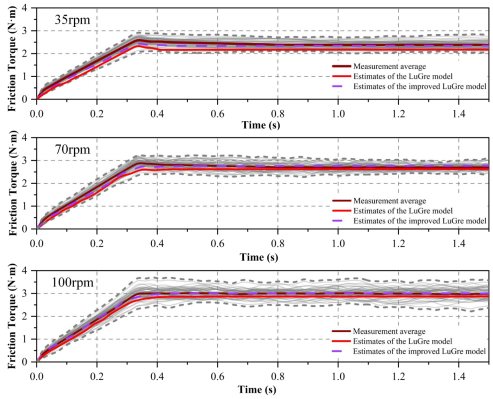

Fig. 4. The experiment is divided into three datasets based on speed: 35 rpm, 70 rpm, and 100 rpm. It presents the average values of measurements and model estimates. Compared to the test average values, the LuGre model estimates exhibit a significant downward bias, indicating the presence of unmodeled variables. Conversely, the improved LuGre model estimates are closer to the measured average values.

fitted as $\bar{\xi} = \{k_0, k_1, k_2, F_C, F_S, v_s\}$. The identification process is mainly carried out through static and dynamic tests [26].

To determine the direction of model improvement, we also need to obtain the uncertainty vector ψ. We assume that the uncertainty model for $\bar{\xi}$ follows a multivariate normal distribution as follows

$$\tilde{\xi}(\bar{\xi}, \mathrm{diag}(\sigma_0^2, \sigma_1^2, \sigma_2^2, \sigma_3^2, \sigma_4^2, \sigma_5^2)) \tag{9}$$

We identify the variances of the dimensions of in a similar manner as described in Section II-A. The parameters employed in our study are analogous to the universal parameters utilized by Konstantinos et al. [27], which have been demonstrated to be effective across many scenarios. The specific parameters are as follows: $\alpha = 0.29$, $\delta = 0.16$, $\varepsilon = 0.29$, $\rho = 0.35$. For the sampling range in the sampling process, we take the 0.95 percentiles of the normal distribution. Through calculations based on (6) and (7), the number of samples for the uncertainty parameters is determined as $n > 7.4$, and we choose $n = 8$. The number of experimental samples is determined as $m > 31.5$, and we choose $m = 50$ to cover the operating range as much as possible. By setting different speeds ω, radial forces f_r, and pressure differences ΔP, a total of 8 types of experiments are

TABLE II
EXPERIMENTAL PARAMETERS FOR STOCHASTIC EXTENSION

	ω(rpm)	f_r(N)	ΔP(Mpa)		ω(rpm)	f_r(N)	ΔP(Mpa)
1	35	25∼35	0.15	5	70	25∼35	0.3
2	35	45∼55	0.15	6	100	25∼35	0.15
3	35	45∼55	0.3	7	100	45∼55	0.15
4	70	25∼35	0.15	8	100	45∼55	0.3

TABLE III
CV OF LUGRE MODEL PARAMETER

	$\psi_{cv}(k_0)$	$\psi_{cv}(k_1)$	$\psi_{cv}(k_2)$	$\psi_{cv}(F_C)$	$\psi_{cv}(F_S)$	$\psi_{cv}(v_s)$
ω=35rpm	17.07	2.05	0.59	0.08	<0.01	0.02
ω=70rpm	26.11	3.05	0.87	0.13	<0.01	0.02
ω=100rpm	41.56	5.05	1.44	0.20	<0.01	0.02

performed. Therefore, a total of 400 experimental setups are conducted, as shown in Table II.

Fig. 4 shows the dataset of the parameter variance identification process, including the mean values and average estimates of the LuGre model. It can be observed that under the condition of keeping other experimental conditions as consistent as possible, the radial force and pressure difference have a significant impact on the joint friction force, and the friction torque after velocity stabilization varies in the range of 2 Nm to 3.5 Nm. This indicates that the special operating conditions of underwater joints have an influence on their friction properties and patterns. By comparing the mean values of the measured test values with the estimated mean values of the LuGre model, it can be observed that there are noticeable errors in the estimates, and they are smaller than the actual measured values. The errors are 3.54%, 5.95%, and 9.95% respectively, which are significantly higher than the estimation errors under normal operating conditions (1.8%). This indicates the need for improvement of the LuGre model in the specific operating conditions of underwater joints. Based on optimization function (5), the model variance is identified using the least squares method, with the variance initially set to 0 and increased by 0.01 at each step until the optimal conditions are reached. The coefficient of variation is calculated using formula (8), and the final results are presented in Table III. There is no significant difference in the data in the two directions of forward and reverse rotation (difference not more than 1%).

From the analysis, the LuGre model's parameters for static friction (F_S) and Stribeck velocity (v_s) exhibit minimal variance, indicating their precise estimation and negating them as priority areas for enhancement. Conversely, the model shows slight uncertainty in Coulomb friction (F_C), suggesting minimal need for refinement. Significant variance in the parameters related to bristle stiffness (k_0) and damping (k_1), which worsens with increasing velocity, highlights these as critical areas for improvement. Additionally, as the velocity increases, the experimental test curves become more scattered, as depicted in Fig. 4. This further indicates that, in the unique operating conditions of underwater joints, friction force is not solely a single-variable function of velocity, as described by the LuGre model. Instead, it is directly related to other factors such as radial force and pressure difference. This suggests the necessity of revisiting and refining variables related to bristle deformation to bolster the LuGre model's accuracy.

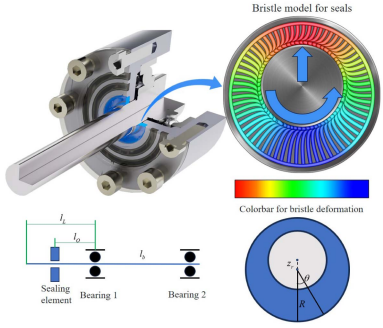

Fig. 5. Schematic diagram of the bristle model and structural diagram.

C. Improvement of the LuGre Model

The LuGre model, used to assess underwater drive joints, faces uncertainty in parameters k_0 (bristle stiffness) and k_1 (bristle damping coefficient). This indicates unmodeled variables in the environment, requiring bristle deformation modeling refinement.

In underwater drive joints, sealing components form a cantilever beam structure, vulnerable to external factors altering contact force with the output shaft, affecting friction. The model, though effective in one-dimensional bristle motion, overlooks radial elastic deformation caused by slight shaft deformation, impacting prediction accuracy.

Underwater pressure changes significantly influence bristle deformation. Unlike land-based joints, underwater joints experience pressure variations with depth, affecting sealing component pre-tightening force and bristle deformation.

Improving the LuGre model involves extending bristle deformation modeling to two dimensions and integrating underwater pressure variables, as depicted in Fig. 5.

Firstly, according to the guidance of the model, the modeling of bristles in the LuGre model is extended to two dimensions. Since underwater joints only undergo minor radial deformation during operation, it can be assumed that the deformation of the bristles is a certain proportionate linear combination of radial and circumferential deformations. Let z_c denote the circumferential deformation, z_r denote the radial deformation, η_1 and η_2 denote the proportionality coefficients, and $\dot{z}_e$ represent the effective deformation velocity of the bristles, as expressed in (10).

$$\begin{aligned}\dot{z}_e &= \eta_1 \dot{z}_c + \eta_2 \dot{z}_r \\ &= \eta_1 (\dot{x} - \frac{k_0 \dot{x}}{g(\dot{x})} z_c) + \eta_2 \dot{z}_r \end{aligned} \tag{10}$$

The parameters η_1 and η_2 in the formula need to be determined by parameter fitting, while $\dot{z}_r$ requires further theoretical modeling. Fig. 5 shows the basic configuration of a conventional underwater drive joint: two bearings ensure the concentricity of the output shaft, ensuring the sealing between the output shaft and the seal, with the distance between the two bearings denoted as l_b. The outward protruding part of the output shaft first contacts the seal, with a distance l_O between the seal and the outer bearing, generating a radial force F_O due to deformation. The end of the output shaft is the actuator, with a gap l_L between it and the outermost bearing, and a load generates a

radial force F_L. To obtain $\dot{z}_r$, the deformation caused by F_L at the position of the seal by the output shaft should be obtained first. Assuming the bending stiffness of the output shaft is E_sI, the deformation z_L caused by F_L at this position without the seal can be obtained through statics analysis according to (11).

$$z_L = \frac{3l_O l_L + 2l_L l_b - l_O^2}{6E_{shaft}I} l_O F_L \tag{11}$$

On the other hand, it is necessary to calculate the relationship between deformation z_r and force F_O. As shown in Fig. 5, the output shaft undergoes slight deformation at the seal due to the load force, causing eccentricity between them. Assuming the seal is an isotropic elastic body, and the deformation is within the range of Hooke's law. Let R be the outer radius of the seal, R_{seal} be the radial thickness, and $\Delta R(\theta)$ be the distance from the contact point in the θ direction to the center of the circle. The radius of the output shaft is r, and the radial deformation at each infinitesimal position can be obtained.

$$\Delta R(\theta) = \frac{r\sin a}{\sin(\pi - \theta)} = \sqrt{r^2 - z_r^2 \sin^2\theta} - z_r \cos\theta \tag{12}$$

Assuming the width of the seal to be B and the Young's modulus to be E_{seal}, integrating around the circumference of the output shaft yields F_O.

$$\begin{aligned} F_O &= \int_0^{2\pi} BRE_{seal} \frac{\Delta R + R_{seal} - R}{R} \cos\theta \mathrm{d}\theta \\ &= BE_{seal}\pi z_r \end{aligned} \tag{13}$$

Hence, we can solve for z_r using (13).

$$\begin{cases} z_L + z_o = z_r \\ F_O = B\pi z_r E_{seal} \end{cases}, z_o = \frac{F_O l_O^2}{3E_{shaft}I}(l_b + l_O) \tag{14}$$

By simplifying (14), we find that z_r is linearly correlated with F_L, from which we can define the proportional coefficient k_L. Thus, we can re-express (10) accordingly.

$$\dot{z}_e = \eta_1 \left(\dot{x} - \frac{k_0 \dot{x}}{g(\dot{x})} z_c \right) + \eta_2 k_L \frac{\mathrm{d}F_L(t)}{\mathrm{d}t} \tag{15}$$

Regarding the pressure difference between the inside and outside, it can be considered to primarily act simultaneously with the radial force and influence Coulomb friction. According to previous research [23], the effects of both can be modeled as linear functions, with proportional coefficients denoted as $k_{C,1}$ and $k_{C,2}$. Thus, we obtain the mathematical model for the improved LuGre model.

$$\begin{aligned} F &= k_0 z + k_1 \dot{z} + k_2 \dot{x} \\ \dot{z} &= \eta_1 (\dot{x} - \frac{k_0 \dot{x}}{g(\dot{x})} z_c) + \eta_3 \frac{\mathrm{d}F_L(t)}{\mathrm{d}t} \\ g(\dot{x}) &= F_C + k_{C,1}\Delta P + k_{C,2} F_L(t) \\ &\quad + (F_S - F_C - k_{C,1}\Delta P - k_{C,2} F_L(t)) e^{-(\dot{x}/v_s)^2} \end{aligned} \tag{16}$$

Where η_3 is the composite coefficient of η_2 and k_L, ΔP represents the internal and external pressure difference, and $F_L(t)$ can be obtained through a priori dynamic model or discrete sensors.

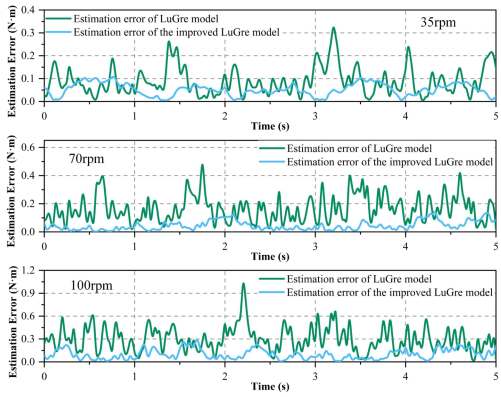

Fig. 6. Comparison of estimation errors between the LuGre model and the improved LuGre model under tests at 35 rpm, 70 rpm, and 100 rpm.

III. Experiment

To validate the effectiveness of the model improvement, we first compare the accuracy of the estimation through model testing in a simulated environment and further assess the superiority of our proposed model at the uncertainty level by applying the cumulative randomness of the model. On the other hand, we tested the compensation effect of the model under typical working conditions in underwater environments, verifying its accuracy and reliability through velocity tracking performance and the ability to reach specified positions.

A. Model Comparison Testing in a Simulated Environment

We used the same method as in Section II-B to identify the parameters of the improved LuGre model. The same dataset containing forward and reverse rotation was used for both experiments, and comparing the estimated means in Fig. 4, it can be seen that the estimated mean of the improved LuGre model better fits the measured mean. For speeds of 35 rpm, 70 rpm, and 100 rpm, the average estimation errors are 2.19%, 1.63%, and 3.31%, respectively, compared to the LuGre model, which decreased by 1.35%, 4.32%, and 6.64%, as shown in Fig. 6.

On the other hand, using the same parameters as in Section II-B, we conduct a stochastic extension of the improved LuGre model. For a more intuitive model comparison, we integrate the added variables and correspond them to the LuGre model, namely comparing $F_C + k_{C,1}\Delta P + k_{C,2}F_L(t)$ with F_C and representing it as $F_{composite}$. As shown in Fig. 7, k_0 (stiffness of bristles) and k_1 (damping coefficient of bristles) as major bristle deformation-related parameters are also the primary improvement targets, with uncertainties decreasing by 49.7% and 55.7%, respectively. Meanwhile, k_2 (viscous friction coefficient) and $F_{composite}$ (Coulomb friction) as secondary optimization items also see decreases in uncertainties by 55.5% and 51.2%.

In addition, we also calculated the cumulative randomness between the two models using formula (8). The cumulative randomness of the LuGre model at three speeds is 19.82, 30.19, and 48.28, respectively, while that of the improved LuGre model is 9.52, 16.55, and 33.54, further proving the effectiveness of the improvement.

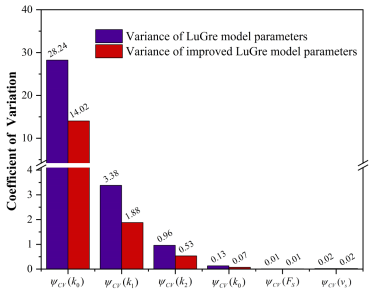

Fig. 7. Comparison of average parameter uncertainties between the LuGre model and the improved LuGre model.

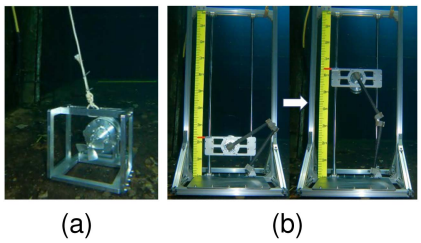

Fig. 8. Comparative testing scenarios of underwater environment models. (a) Propeller testing platform. (b) Single-joint-driven leg testing platform.

B. Model Comparison Testing in Underwater Environments

To further validate our proposed method's efficacy, we conducted verification experiments on the joints detailed in Section II, within a 3.5-meter-deep pool. These experiments encompassed three distinct groups: velocity tracking tests, low-speed stability tests, and, mirroring typical operational scenarios for underwater robot joints, as illustrated in Fig. 8. We separately integrated both the standard LuGre model and our enhanced version into the joint driver control board, accounting for additional friction induced by seals during current output. Given the challenges of accurately measuring real-time friction at seal positions underwater, and the potential introduction of unmodeled variables and disturbances by additional underwater sensor components, our experiments focused on velocity or position modes. This approach allowed us to compare the compensation effects of the two models through their velocity tracking performance or ability to attain specified positions.

1) In the velocity tracking test, we attached small propellers to the joint output shaft to simulate rotational loads, similar to those experienced by underwater robots using thrusters (see Fig. 8(a)). The joint's velocity was sinusoidally varied between 65 rpm and 95 rpm, with a 5-second period. Fig. 9(a) shows the results, omitting the initial acceleration phase for clarity. The LuGre model's compensation struggled to keep up with the expected velocity curve due to factors like water depth. It eventually synchronized with the command velocity cycle, but the velocity error persisted until 25 seconds (Fig. 9(b)). On the other hand, the enhanced LuGre model, with added friction compensation for factors such as water depth, quickly and accurately tracked the command velocity curve. It achieved an 89% reduction in velocity error compared to the standard LuGre model from 0.15 s to 25 s.

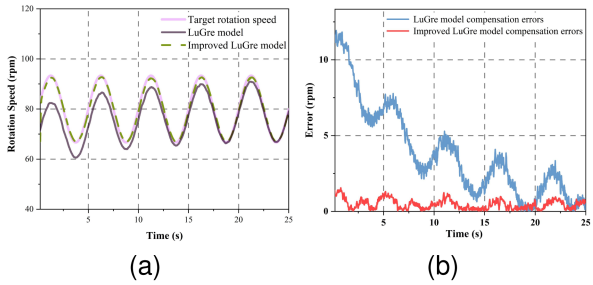

Fig. 9. Velocity tracking tests under model compensation. (a) Comparison of velocity tracking curves. (b) Comparison of velocity tracking errors.

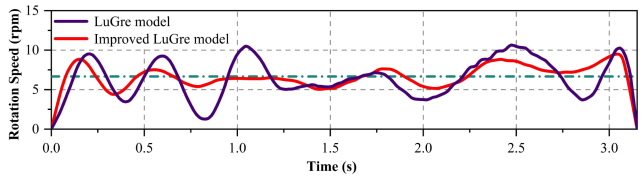

Fig. 10. Velocity curve of low-speed stability test.

This validates the enhanced model's superior response speed and tracking performance under loaded underwater conditions, confirming the effectiveness of our improvement approach.

2) For the low-speed stability test, we used a single-joint-driven leg testing platform (Fig. 8(b)) to mimic the vertical motion of a legged robot's single leg with a solitary joint drive rod. The joint lifted a 2 kg underwater weight at a constant 6.6 rpm. Crawling phenomena were evident around 6 rpm (Fig. 3(b)), demanding precise compensation. The radial force change curve required by the improved LuGre model was obtained through ADAMS simulation. Due to difficulties in characterizing underwater joint friction accurately, the LuGre model exhibited significant velocity fluctuations, including prolonged oscillations lasting up to 1.25 s at motion initiation, and a sudden drop in speed around 2.7 s, which is shown in Fig. 10. In contrast, the enhanced LuGre model experienced only 0.5 s of initial oscillations due to speed overshoot, followed by minor post-stabilization fluctuations. The average error rate dropped from 34.2% with the LuGre model to 18.7% with the enhanced model, validating its effectiveness in handling nonlinear friction variations like crawling and stick-slip.

3) For the impact load test, we used the same setup as the low-speed stability test. Both the enhanced LuGre model and the standard LuGre model underwater joints were tasked with reaching specified positions at identical maximum speeds and accelerations to enable the legged platform's jumping functionality. Due to the radial impact force generated during jumping, which results from leg propulsion, the compensation model needed to respond quickly and robustly.

Fig. 11 compares the position data of the two models. Clearly, the enhanced LuGre model achieves the target position faster, in just 0.311 s compared to the LuGre model's 0.529 s, with smoother position changes. Despite the higher speed, the enhanced LuGre model avoids significant position overshoot. This test highlights the model's improved robustness and operational versatility achieved through stochastic expansion.

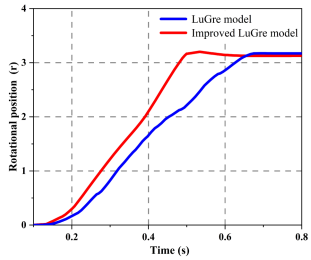

Fig. 11. Impact load test position change curve.

IV. Conclusion

This letter proposes a direction-guided improvement method for the LuGre model and applies it to the model improvement of sealed joints for underwater robotics. This method obtains parameter confidence through random expansion of the model, ranks the degree of optimizability, and effectively guides the improvement direction of the LuGre model under special conditions. Applying this method, we improved the model of underwater sealed joints based on the LuGre model, expanded the brush model from one dimension to two dimensions under the guidance of random expansion methods, and increased consideration of the influence of water depth. Through simulated environmental tests, we obtained that the estimation errors of the improved model decreased by 1.35%, 4.32%, and 6.64% respectively under low-speed, medium-speed, and high-speed conditions. The effectiveness of the improvement method and the improved model was verified through three tests: velocity tracking, low-speed stability, and impact load tests in real underwater environments.

In future work, we will continue to evaluate the proposed method and study how to further improve the accuracy by incorporating other physical phenomena (such as fluid viscosity). Additionally, we are working towards applying the model to complete robot prototypes.

References

[1] F. E. Fish, "Advantages of aquatic animals as models for bio-inspired drones over present," *AUV Technol. Bioinspiration Biomimetics*, vol. 15, no. 2, Mar. 2020, Art. no. 025001.

[2] G. Rill, T. Schaeffer, and M. Schuderer, "LuGre or not LuGre," *Multibody Syst. Dyn.*, vol. 60, no. 2, pp. 191–218, Feb. 2024.

[3] H. Liu, B. Yang, C. Wang, Y. Han, and D. Liu, "The mechanisms and applications of friction energy dissipation," *Friction*, vol. 11, no. 6, pp. 839–864, Jun. 2023.

[4] A. Mashayekhi, S. Behbahani, A. Nahvi, M. Keshmiri, and M. Shakeri, "Analytical describing function of LuGre friction model," *Int. J. Intell. Robot. Appl.*, vol. 6, no. 3, pp. 437–448, Sep. 2022.

[5] A. Mashayekhi, M. Shakeri, S. Behbahani, and M. Keshmiri, "Describing function of the Gaussian friction model and its effect on stability of a haptic device," *J. Braz. Soc. Mech. Sci. Eng.*, vol. 46, no. 3, Mar. 2024, Art. no. 166.

[6] G. Quaranta, W. Lacarbonara, and S. F. Masri, "A review on computational intelligence for identification of nonlinear dynamical systems," *Nonlinear Dyn.*, vol. 99, no. 2, pp. 1709–1761, Jan. 2020.

[7] K. J. Astrom and C. Canudas-de-wit, "Revisiting the LuGre friction model," *IEEE Control Syst. Mag.*, vol. 28, no. 6, pp. 101–114, Dec. 2008.

[8] S. Han, G. Orzechowski, J.-G. Kim, and A. Mikkola, "Data-driven friction force prediction model for hydraulic actuators using deep neural networks," *Mechanism Mach. Theory*, vol. 192, Feb. 2024, Art. no. 105545.

[9] M. Iskandar and S. Wolf, "Dynamic friction model with thermal and load dependency: Modeling, compensation, and external force estimation," in *Proc. IEEE Int. Conf. Robot. Automat.*, 2019, pp. 7367–7373.

[10] J. Li, Y. Lu, F. He, and L. Miao, "Motion control of hydraulic actuators with nonlinear friction compensation: Applied to variable valve systems of diesel engine," *ISA Trans.*, vol. 137, pp. 561–573, Jun. 2023.

[11] T. T. Paulsen, I. F. Santos, and L. K. H. Clemmensen, "Contribution to the estimation of force coefficients of plain gas seals with high preswirl considering rotor-foundation dynamics," *Mech. Syst. Signal Process.*, vol. 186, Mar. 2023, Art. no. 109885.

[12] M. H. Mueser and L. Nicola, "Modeling the surface topography dependence of friction, adhesion, and contact compliance," *MRS Bull.*, vol. 47, no. 12, pp. 1221–1228, Dec. 2022.

[13] G. Picardi, M. Chellapurath, S. Lacoponi, S. Stefanni, C. Laschi, and M. Calisti, "Bioinspired underwater legged robot for seabed exploration with low environmental disturbance," *Sci. Robot.*, vol. 5, no. 42, May 2020, Art. no. eaaz1012.

[14] T. Kim, J. Kim, and S.-C. Yu, "Development of bioinspired multimodal underwater robot "HERO-BLUE" for walking, swimming, and crawling," *IEEE Trans. Robot.*, vol. 40, pp. 1421–1438, 2024.

[15] X. Ma, G. Wang, and K. Liu, "Design and optimization of a multimode amphibious robot with propeller-leg," *IEEE Trans. Robot.*, vol. 38, no. 6, pp. 3807–3820, Dec. 2022.

[16] H. Dong, Z. Ji, Y. Meng, D. Chen, T. Qiao, and J. Yu, "Water entry locomotion strategy for a stranding bionic robotic fish," *J. Field Robot.*, 2024, doi: 10.1002/rob.22352.

[17] A. Cavallo, M. Costanzo, G. De Maria, and C. Natale, "Modeling and slipping control of a planar slider," *Automatica*, vol. 115, May 2020, Art. no. 108875.

[18] K. Dai et al., "Adaptive force tracking control of electrohydraulic systems with low load using the modified LuGre friction model," *Control Eng. Pract.*, vol. 125, Aug. 2022, Art. no. 105213.

[19] L. Zhang, H. Tang, T. Sun, J. Yu, Z. Li, and X. Wang, "Vibration characteristics analysis of shaft system for bulb hydroelectric generating unit based on magnetorheological fluid damper," *Chaos Solitons Fractals*, vol. 163, Oct. 2022, Art. no. 112559.

[20] H. Wang and P. G. Leaney, "A new friction model in hybrid pump-controlled asymmetric (single-rod) cylinder drive system," *Tribology Trans.*, vol. 63, no. 5, pp. 867–878, Jul. 22, 2020.

[21] C. Zhang, W. Sun, Y. Cheng, B. Wang, Z. Wang, and Y. Wang, "Investigations on bearing performances of metal rubber-bump foil gas journal bearing with three structure pads integrating stiffness and damping," *Tribology Int.*, vol. 188, Oct. 2023, Art. no. 108816.

[22] P. Soleimanian and H. Ahmadian, "Modeling friction effects in lubricated roller guideways using a modified LuGre model," *J. Vib. Control*, vol. 28, no. 19–20, pp. 2519–2530, Oct. 2022.

[23] F. Marques, L. Wolinska, M. Wojtyra, P. Flores, and H. M. Lankarani, "An investigation of a novel LuGre-based friction force model," *Mechanism Mach. Theory*, vol. 166, Dec. 2021, Art. no. 104493.

[24] L. Simoni, M. Beschi, A. Visioli, and K. J. Astrom, "Inclusion of the dwell time effect in the LuGre friction model," *Mechatronics*, vol. 66, Apr. 2020, Art. no. 102345.

[25] L. Colantonio, P. Dehombreux, M. Hajzman, and O. Verlinden, "3D projection of the LuGre friction model adapted to varying normal forces," *Multibody Syst. Dyn.*, vol. 55, no. 3, pp. 267–291, Jul. 2022.

[26] P. Aivaliotis, D. Kaliakatsos-Georgopoulos, and S. Makris, "Physics-based modelling of robot's gearbox including non-linear phenomena," *Int. J. Comput. Integr. Manuf.*, vol. 36, no. 12, pp. 1864–1875, Dec. 02, 2023.

[27] K. Karydis, I. Poulakakis, J. Sun, and H. G. Tanner, "Probabilistically valid stochastic extensions of deterministic models for systems with uncertainty," *Int. J. Robot. Res.*, vol. 34, no. 10, pp. 1278–1295, Sep. 2015.

[28] M. Vidyasagar, "Randomized algorithms for robust controller synthesis using statistical learning theory," *Automatica*, vol. 37, no. 10, pp. 1515–1528, Oct. 2001.

[29] M. Vidyasagar, *Learning and Generalization: With Applications to Neural Networks*. Berlin, Germany: Springer Sci. Bus. Media, 2013.